Chapter 15
Ultrasound in the Neurointensive Care Unit

Venkatakrishna Rajajee

Introduction

Bedside ultrasound has long played an important role in the neurointensive care unit, although mostly in the form of transcranial Doppler (TCD) for the detection of cerebral vasospasm following subarachnoid hemorrhage (SAH) [1]. More recently, however, the range of potential clinical applications for bedside ultrasound in the neurointensive care unit has greatly expanded. Optic nerve ultrasound (ONUS) has been extensively investigated as a noninvasive tool for the detection of raised intracranial pressure (ICP) [2–6]. Similar to patients in any other unit, bedside ultrasound is also invaluable for the assessment of shock, acute hypoxic respiratory failure, suspected deep venous thrombosis, and for the performance of several common bedside procedures. Patients with aneurysmal subarachnoid hemorrhage (aSAH) may particularly benefit from the use of bedside ultrasound: in addition to the risk of cerebral vasospasm, they are at considerable risk for severe left ventricular dysfunction and neurogenic pulmonary edema. While cranial ultrasound in the neonate and carotid ultrasound in ischemic cerebrovascular disease are among the most common applications of ultrasound relevant to neurological disease, they are beyond the scope of this chapter, which will focus on common applications of multipurpose point-of-care (POC) ultrasound in the adult neurointensive care unit.

V. Rajajee, M.D. (✉)
Departments of Neurosurgery & Neurology, University of Michigan Health System,
3552 Taubman Health Care Center, SPC 5338, 1500 E. Medical Center Drive,
Ann Arbor, MI 48109-5338, USA
e-mail: vrajajee@yahoo.com

M. Jankowich, E. Gartman (eds.), *Ultrasound in the Intensive Care Unit*,
Respiratory Medicine, DOI 10.1007/978-1-4939-1723-5_15

Transcranial Color-Coded Sonography

Technical and Patient Considerations

Transcranial Doppler vs Transcranial Color-Coded Sonography

Transcranial Doppler sonography has traditionally been performed using dedicated portable machines and transducers that display a spectral Doppler waveform only. Acquisition of the Doppler signal from intracranial vessels with these machines requires "blind" manipulation of the probe and adjustment of depth of the sample volume. "Blind" TCD can therefore be technically challenging, particularly for inexperienced operators. While traditional TCD is an established and well-validated tool, this technique requires dedicated equipment separate from the multipurpose point-of-care machines typically available in the intensive care unit (ICU). The angle of insonation of vessels cannot be known, and an insonation angle of greater than 60° may easily occur, leading to marked inaccuracy in measured velocities.

Transcranial color-coded sonography (TCCS) is performed using multipurpose machines with standard phased array probes to obtain grayscale images of cerebral parenchyma and duplex images of intracranial vessels, permitting rapid acquisition and identification of multiple intracranial vessels. The pulse Doppler spectral waveform is obtained guided by the duplex images, with appropriate consideration for the angle of insonation. More recently, TCCS capability in hand-carried POC ultrasound machines more familiar to intensive care professionals has become more widely available, obviating the need for dedicated TCD equipment. Image-guided acquisition of Doppler waveforms with TCCS can be much easier than "blind" acquisition of Doppler signal using traditional TCD, particularly for trainees and inexperienced sonographers. For these reasons, this chapter will focus on the use of TCCS instead of "blind" TCD. Potential disadvantages of TCCS are the relatively larger footprint of the probe and the relative insensitivity of duplex ultrasound for low flow signals.

Equipment

A phased array (5–1 MHz) transducer (Fig. 15.1) is used, and the transcranial preset (Fig. 15.2) selected. Transcranial imaging cannot be performed with the cardiac and abdominal presets available on most multipurpose POC machines.

Patient Factors

The patient is positioned supine with the head resting comfortably back on the bed during transtemporal insonation. During transforaminal insonation the patient is ideally positioned sitting up with the head flexed forward; however, the patient can also be positioned on his/her side with the chin in contact with the chest. While no specific adverse effects have been reported with the diagnostic use of standard

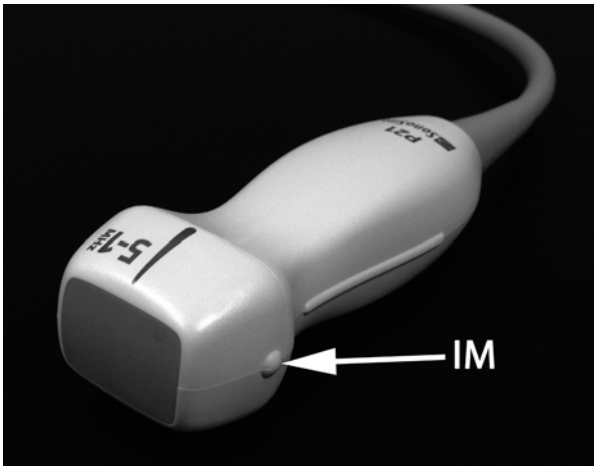

Fig. 15.1 Phased array transducer used for TCCS. *IM* index mark on the probe corresponds to index mark on the screen

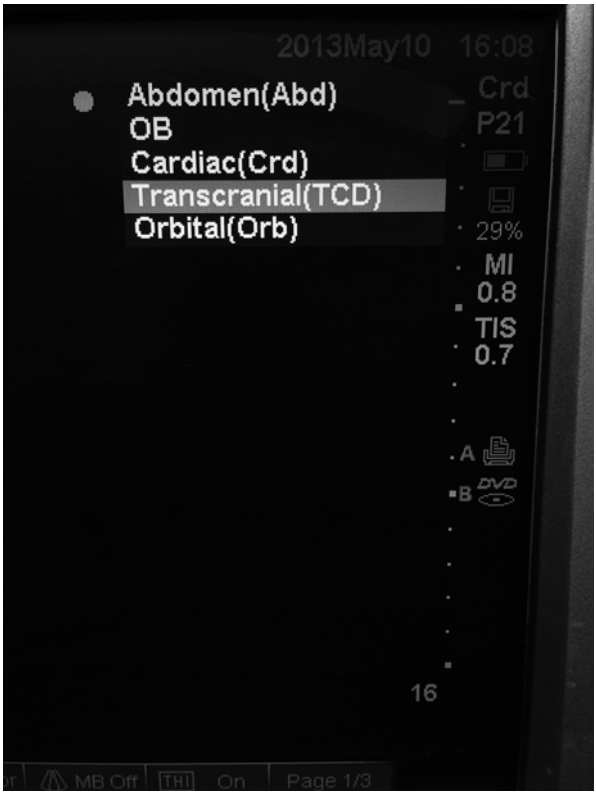

Fig. 15.2 Selection of transcranial preset. Select "Transcranial" from the l ist of presets available for the phased array transducer probe

TCD/TCCS probes, the general principle of ALARA (as low as reasonably achievable) must be kept in mind, with the duration of insonation restricted to that which is clinically essential. This is particularly true because transcranial insonation typically requires maximal acoustic power output. About 5–20 % of patients have an inadequate transtemporal window for performance of TCCS [7, 8]. Risk factors for absence of transtemporal window include older age, female sex, and measured skull thickness [7, 8].

Image Acquisition and Interpretation

Image Acquisition

The sector-shaped image on the screen obtained from the phased array probe is oriented with the index mark on the upper left aspect of the image. The examiner ideally stands behind the patient's head, although any position that allows the elbow to rest on the patient's bed or be held close to the examiner's side is acceptable; arm fatigue can be expected to develop rapidly. Insonation is initially performed through the transtemporal acoustic window, with the transducer placed immediately anterior to the upper border of the tragus and superior to the posterior zygomatic arch (Fig. 15.3). The index mark on the probe is directed anteriorly and rotated at a 10–20° angle superior to the axial plane (Fig. 15.4) with the transducer itself tilted at a 10–20° angle cephalad to the axial plane (Fig. 15.5). If the desired image is not obtained, the probe can be moved within the approximate area delineated by the circle in Fig. 15.3 until the desired initial grayscale image is obtained. If no recognizable anatomical features are seen, it is possible that the patient does not have an acoustic window on that side.

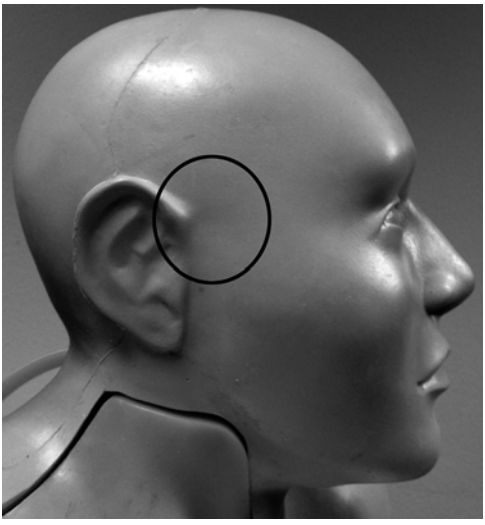

Fig. 15.3 Transtemporal window. The phased array probe can be moved within the *circle* until the midbrain is identified on B-mode

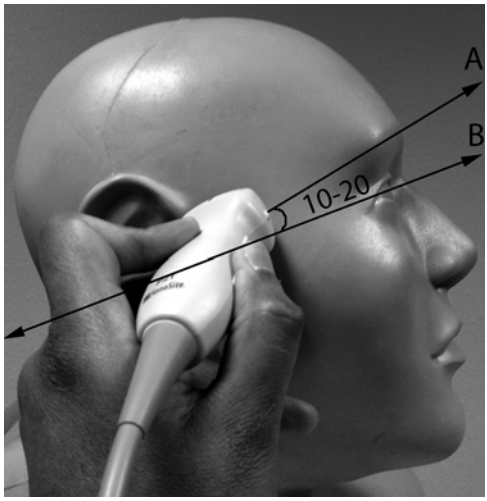

Fig. 15.4 Probe position for TCCS – lateral view of transtemporal insonation. The transducer is rotated slightly so the index mark on the phased array probe points in the direction A, which is at about a 10–20° angle to the anatomical axial plane, depicted by line B

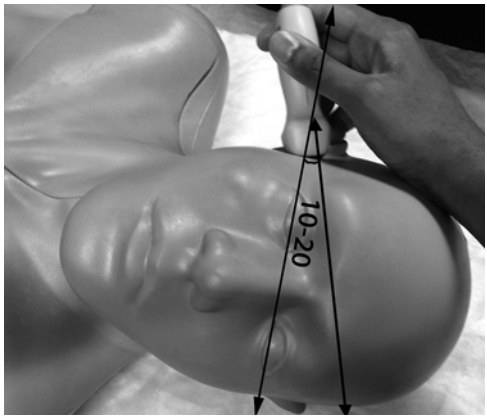

Fig. 15.5 Probe position for TCCS – anteroposterior view of transtemporal insonation. The transducer is tilted slightly cephalad, at a 10–20° angle to the anatomical axial plane

The single most important anatomical feature to identify at this point is the *midbrain* (Fig. 15.6), at a depth of about 5–8 cm, with the "Mickey Mouse ears" of the crus cerebri seen turned on their side. This is comparable, but not identical, to the image obtained with computed tomography (CT) imaging at this level (Fig. 15.7). Once this plane of imaging is obtained, other prominent anatomical features can be rapidly identified, including the *lesser sphenoid wing of the temporal bone* and the *basal cisterns*, particularly the interpeduncular and quadrigeminal cisterns (Figs. 15.6 and 15.7). The normal anatomical distribution of the major intracranial arteries and the circle of Willis is shown in Fig. 15.8. Once the midbrain is identified on the grayscale image, the color box is positioned over the expected anatomical location of the vessel(s) of interest, with "red" typically depicting flow toward and "blue" flow away from the probe. The most important intracranial artery to identify

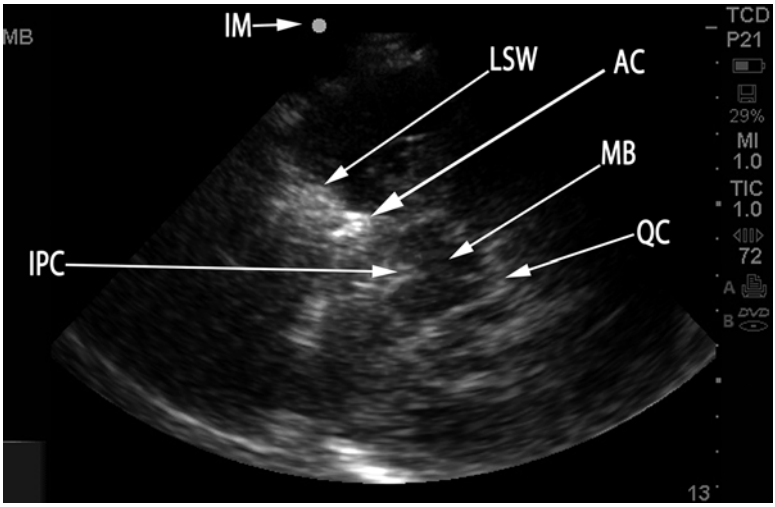

Fig. 15.6 B-mode image at level of the midbrain. Compare to Fig. 15.7, which depicts CT imaging at the same level in the same aSAH patient, with the same anatomical features labeled. *IM* index mark (corresponds to Index Mark on transducer), *MB* midbrain, *LSW* lesser sphenoid wing, *AC* aneurysm clip, *QC* quadrigeminal cistern, *IPC* interpeduncular cistern

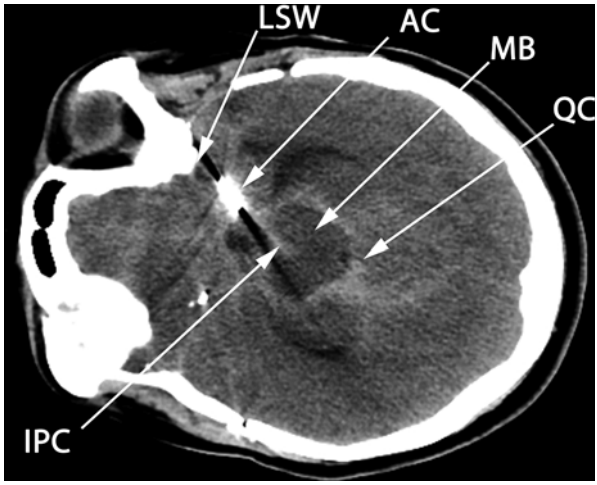

Fig. 15.7 CT axial image at level of midbrain. Compare to Fig. 15.6, which depicts B-mode image at the same level in the same aSAH patient, with the same anatomical features labeled. The CT image has been rotated 90° to the *left* for easier comparison to the ultrasound image. *MB* midbrain, *LSW* lesser sphenoid wing, *AC* aneurysm clip, *QC* quadrigeminal cistern, *IPC* interpeduncular cistern

is the *middle cerebral artery (MCA)*, seen as a curved vessel extending out toward the probe with flow directed toward the probe (depicted in red in Fig. 15.9) from a point anterior and lateral to the midbrain that is the point of bifurcation of the internal carotid artery, at about 4–6 cm depth. The A1 segment of the *anterior cerebral artery* (ACA) is seen extending from the *internal carotid artery* (ICA) bifurcation in the opposite direction, anteriorly, and toward the midline, with flow away from

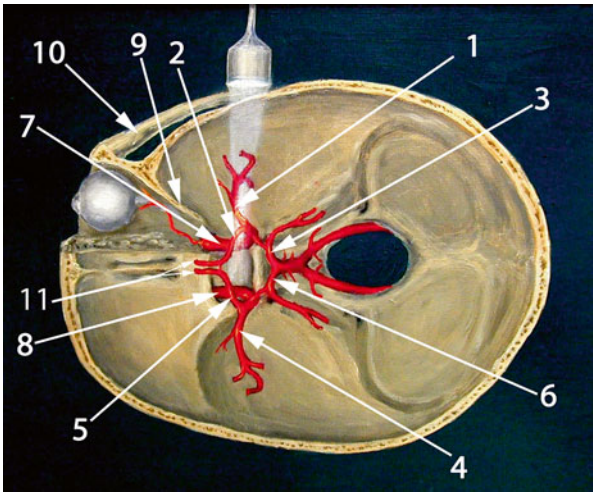

Fig. 15.8 Normal anatomical distribution of intracranial arteries. Compare to Fig. 15.9, which is a duplex image of the circle of Willis in approximately the same anatomical plane with the same labeling. *1* Ipsilateral MCA, *2* ipsilateral ACA A1 segment, *3* ipsilateral PCA P1 segment, *4* contralateral MCA, *5* contralateral ACA A1 segment, *6* contralateral PCA P1 segment, *7* ipsilateral ICA, *8* contralateral ICA, *9* lesser sphenoid wing, *10* zygomatic arch, *11* bilateral ACA A2 segments (This figure was adapted from http://en.wikipedia.org/wiki/File:Transcranial_doppler.jpg under the terms of GNU Free Documentation License, Version 1.3 by Rune Aaslid)

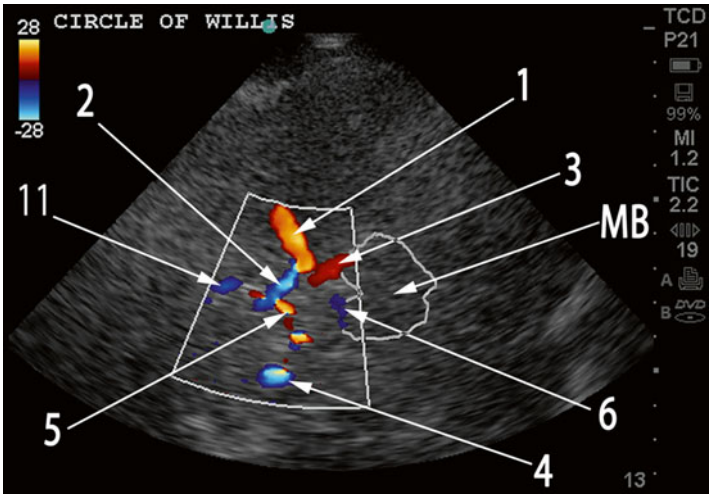

Fig. 15.9 TCCS duplex image of the circle of Willis. Compare to Fig. 15.8 which depicts normal anatomical distribution of intracranial vessels in approximately the same anatomical plane with the same labeling. *1* ipsilateral MCA, *2* ipsilateral ACA A1 segment, *3* ipsilateral PCA P1 segment, *4* contralateral MCA, *5* contralateral ACA A1 segment, *6* contralateral PCA P1 segment, *11* bilateral ACA A2 segments (cannot be distinguished on TCCS)

the probe (depicted in blue in Fig. 15.9). The ipsilateral (blue) and contralateral (red) A1 segments appear to meet in the midline (where the anterior communicating artery is typically *not* visualized) with the two A2 segments (which can often not be individually distinguished) extending anteriorly from this point, in the midline, with flow away from the probe (blue in Fig. 15.9). Minimal downward (caudal) angulation of the probe from this plane will reveal the distal internal carotid artery (ICA) following its entry into the skull, in continuity with proximal MCA, with flow directed toward the probe. Placing the color box around the midbrain itself, in the original plane of insonation, will reveal the *posterior cerebral artery* (PCA) curving around the crus cerebri and the midbrain from its point of origin (the bifurcation of the basilar artery) in the interpeduncular cistern. The ipsilateral PCA P1 segment demonstrates flow toward the probe (red in Fig. 15.9), which changes to flow away from the probe (blue) in the P2 segment following the completion of the bend in the PCA around the crus cerebri.

Increasing the depth of insonation to 13 cm or greater and extending the color box will sometimes reveal the contralateral intracranial vessels, depending on the quality of the acoustic window. This is most feasible when performing insonation through a large decompressive craniectomy defect. When visible, the contralateral ACA A1 segment and PCA P2 segments are seen with flow toward the probe (red), while the contralateral MCA and PCA P1 segment are seen with flow away from the probe (blue), as seen in Fig. 15.9. An attempt at interrogation of the contralateral vessels may be the only recourse when a patient has a viable transtemporal acoustic window on only one side.

To visualize the vertebrobasilar circulation, the patient's head is flexed forward and the transducer firmly positioned in the suboccipital region with use of copious conductive gel to permit acoustic transmission through the hair at the nape of the neck. The probe is angled so that the long axis of the probe passes through the *nasion*, permitting insonation through the foramen magnum (Fig. 15.10). The most important structure seen on the grayscale image will be the *foramen magnum*, a large circular hypoechoic structure in the midline between about 2–7 cm of depth (Fig. 15.11). The color box is placed so that it covers the foramen magnum and the

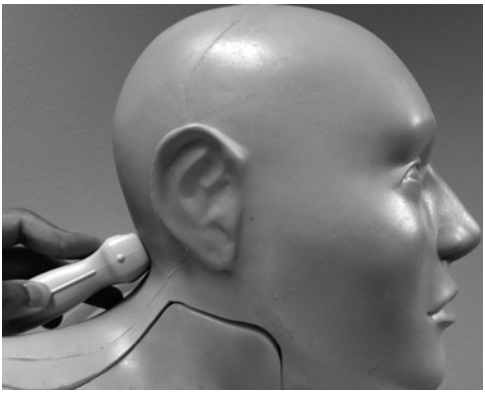

Fig. 15.10 Probe position for TCCS – transforaminal (suboccipital) window. Probe is placed below occipital protuberance with head flexed (head flexion not demonstrated in this image), probe points toward the nasion

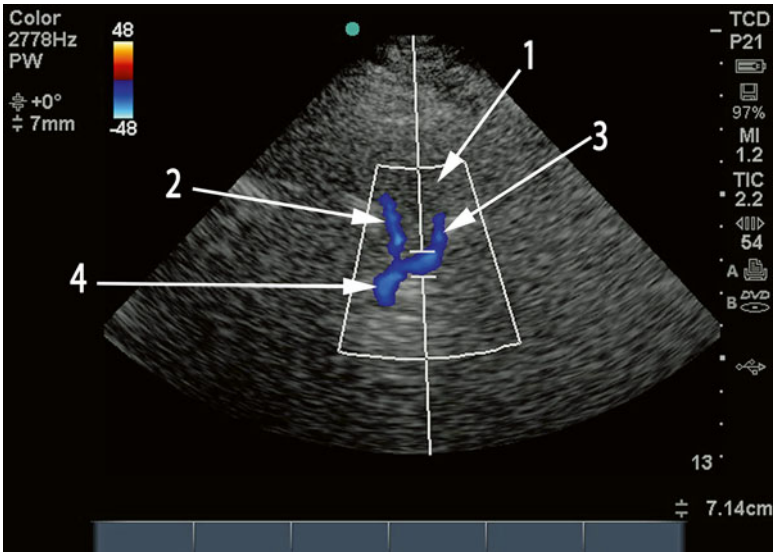

Fig. 15.11 Transforaminal view of vertebral and basilar arteries. The hypoechoic circular structure labeled 1 is the foramen magnum. *Right* (*2*) and *left* (*3*) vertebral arteries meet to form the basilar artery (*4*), producing the characteristic Y shape on duplex imaging

expected location of the *basilar artery* deeper to the foramen, within the cranial vault. The two *vertebral arteries* are visualized on either side of the foramen magnum, with flow away from the probe (blue in Fig. 15.11), extending intracranially to a point of confluence at about 6–8 cm of depth, beyond which the basilar artery is seen extending distally into the cranial vault, also with flow away from the probe (blue in Fig. 15.11). This confluence typically results in the "Y" shape seen in Figs. 15.11 and 15.12. The distal bifurcation of the basilar artery is typically not visualized with TCCS.

Once the vessels of interest are identified, pulse Doppler is selected with a sample volume size of about 3–10 mm. The sample volume is then placed on the arterial segment of interest (Fig. 15.13). Since the anatomical orientation of the artery can be clearly visualized, an effort must be made to obtain an insonation angle as close as possible to zero degrees for flow toward the probe and 180° for flow away from the probe (Figs. 15.13 and 15.14). When this is not possible, most POC machines with TCCS capability permit angle correction through manual delineation of the direction of flow within the vessel. The machine then corrects the calculated velocity using a formula that includes the angle of insonation. Using angle correction is generally not recommended when the angle of insonation is greater than 60° or when a sufficiently long arterial segment is not available to accurately depict the direction of flow. Once the sample volume is appropriately positioned (and angle correction performed if so desired), the spectral Doppler reading is obtained (Fig. 15.15). The Doppler frequency shift recorded within the sample volume is converted to flow velocity, depicted on the y-axis, against time, on the x-axis.

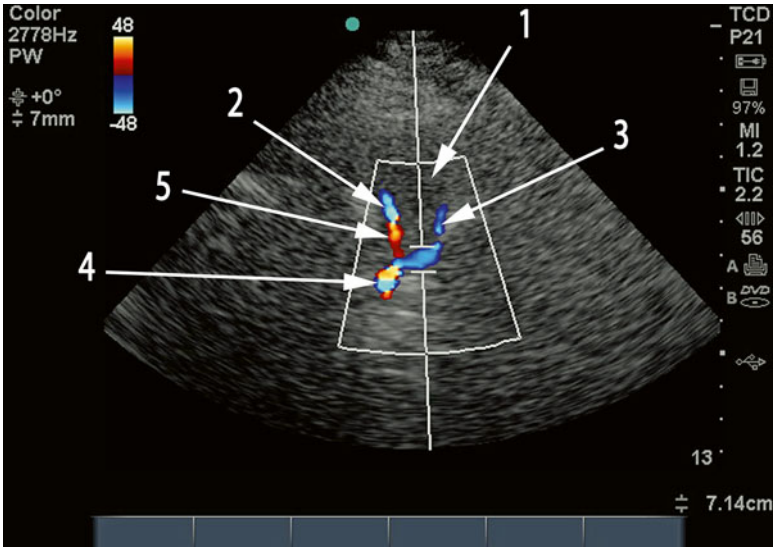

Fig. 15.12 Aliasing in the vertebrobasilar circulation. Repeat TCCS performed on the same patient with aSAH several days following Fig. 15.11. Identical image to Fig. 15.11, except aliasing is seen in the distal right vertebral (*5*) and proximal basilar (*4*) arteries. *1* foramen magnum, *2* right vertebral artery with aliasing in the distal segment labeled 5, *3* left vertebral artery, *4* basilar artery now with aliasing

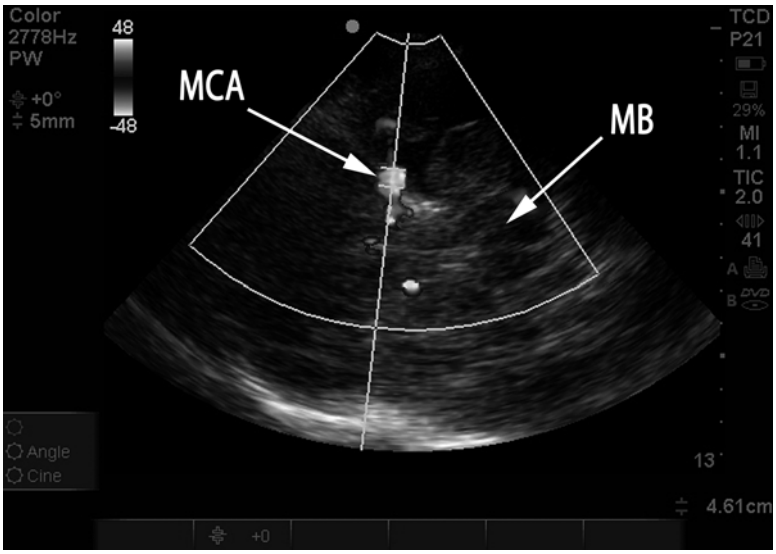

Fig. 15.13 Placement of sample volume on MCA, good angle of insonation. Duplex color image rendered in *black* and *white*. The sample volume has been placed in the MCA M1 segment. Note excellent angle of insonation, in-line with direction of flow in the MCA. *MB* midbrain, *MCA* middle cerebral artery

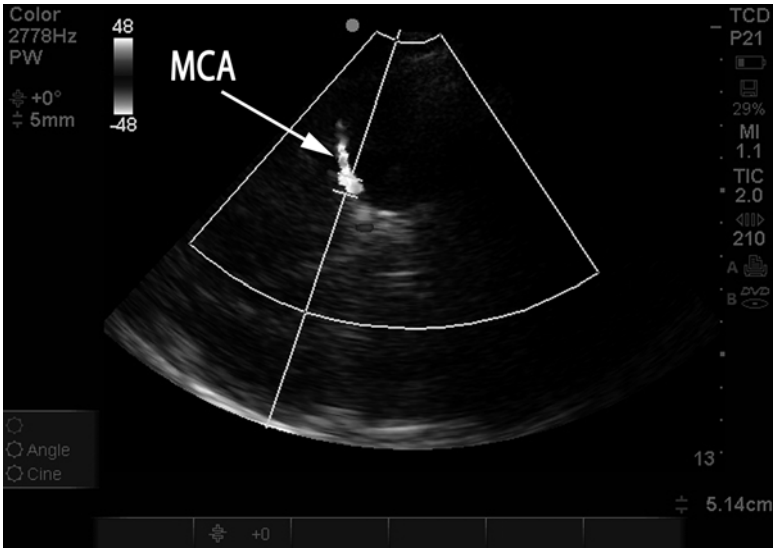

Fig. 15.14 Placement of sample volume on MCA, suboptimal angle of insonation. Duplex color image rendered in *black* and *white*. Same patient and examination as in Fig. 15.13. Probe has been moved slightly and the sample volume is again placed on the MCA M1 segment; however, there is now a relatively steep angle of insonation to the direction of flow in the MCA, which will artificially lower the measured mCBFV. Probe position needs to be altered slightly to optimize angle of insonation, seen in Fig. 15.13

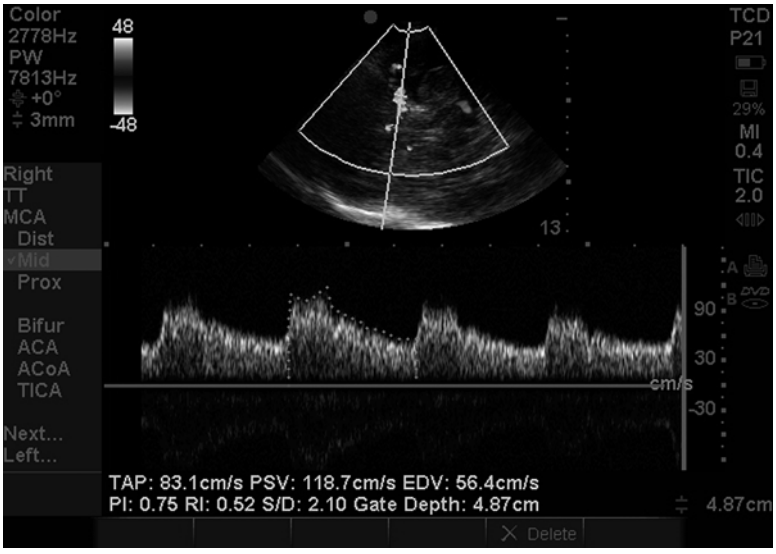

Fig. 15.15 Spectral Doppler waveform. Spectral Doppler waveform obtained from sample volume placement on MCA shown in Fig. 15.13. The mCBFV is depicted here as the time averaged peak (TAP). *PSV* peak systolic velocity, *EDV* end-diastolic velocity, *PI* pulsatility index

One complete cardiac cycle on the spectral Doppler waveform is then traced out and the machine calculates the parameters of interest, including the peak systolic velocity (PSV), end-diastolic velocity (EDV), the mean cerebral blood flow velocity (mCBFV – otherwise known as the time averaged peak or TAP), and the pulsatility index {PI = (PSV-EDV)/mean flow velocity or MFV}.

When the blood flow velocity within an arterial segment is relatively high relative to the set color scale, aliasing may occur. Aliasing is visible as an abrupt change in color duplex examination within a segment of the artery (but not the entire artery) from the expected color appropriate to the direction of flow to the opposite color: red to blue or vice versa. The presence of aliasing can be clinically useful, since regions of aliasing are more likely to represent higher velocities and can be preferentially sampled when looking for vasospasm (Fig. 15.12). Most aliasing does NOT represent vasospasm; however, and if so desired, aliasing can be eliminated by increasing the range of the color scale.

Once the intracranial vessels have been interrogated, measuring the velocities in the distal cervical internal carotid arteries, immediately prior to their entry into the skull, should be performed when evaluating for vasospasm. These extracranial ICA (exICA) velocities are used to calculate the *Lindegaard ratio* ($mCBFV_{MCA}/mCBFV_{exICA}$). The transducer is placed in the submandibular region at the angle of the jaw and directed upward and slightly medially, toward the ipsilateral eye (Fig. 15.16). The exICA is a linear (sometimes tortuous) vessel with flow away from the probe (blue in Fig. 15.17) and is typically medial to the internal jugular vein, which is distinguished by the presence of flow toward the probe (red) and a venous pattern of pulsation. The most important distinguishing feature of the exICA, compared to the

Fig. 15.16 Probe position for TCCS – submandibular insonation. Probe is placed below angle of the jaw and directed upward and slightly medially

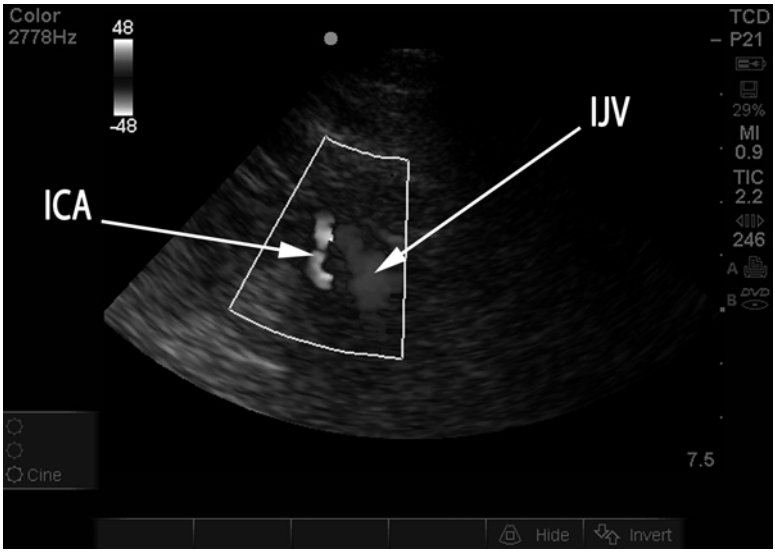

Fig. 15.17 Extracranial ICA and IJV seen on submandibular insonation. Duplex color image rendered in *black* and *white. ICA* internal carotid artery, was *blue* in original duplex image depicting flow away from probe. *IJV* internal jugular vein, was *red*, with flow toward the probe

external carotid artery, is the presence of substantial diastolic flow in the exICA. As with intracranial vessels, obtaining an angle of insonation as close to 0° or 180° as possible is important; otherwise, perform angle correction.

Image Interpretation

The most important parameter obtained from TCCS is the mCBFV, since most angiographic correlation to vessel caliber has been performed with this parameter. The range of "normal" velocities used at the University of Michigan is shown in Table 15.1.

1. Cerebral vasospasm after aSAH
   Reduction in vessel caliber caused by cerebral vasospasm following aSAH will result in an elevation in mCBFV, since velocity of blood flow is inversely proportional to the square of the vessel radius [9]. A mCBFV <120 cm/s in the MCA is reliable for the exclusion of hemodynamically significant vasospasm and mCBFV >200 cm/s is specific for severe vasospasm [1, 10]. Elevations in velocity between 120 and 200 cm/s may be caused by either hyperdynamic flow or vasospasm. Hyperdynamic flow frequently results from factors such as the catecholamine surge following aSAH, anxiety, pain, fever, anemia, and the use of inotropic agents. The Lindegaard ratio ($mCBFV_{MCA}/mCBFV_{exICA}$) can be used to differentiate hyperdynamic flow from vasospasm [1, 10]. A ratio >3 likely

Table 15.1 Normal range of mean cerebral blood flow velocities

Intracranial artery	Normal range of mCBFV (cm/s)
Middle cerebral artery (MCA)	37–81
Anterior cerebral artery (ACA)	25–77
Posterior cerebral artery (PCA)	18–58
Intracranial internal carotid artery (ICA)	19–69
Vertebral artery	16–56
Basilar artery	21–57
Extracranial internal carotid artery (ExICA)	28–48

represents mild vasospasm and a ratio >6 severe vasospasm. Thresholds for the identification of vasospasm have been validated primarily in the MCA. However, normal MCA velocities are almost always higher than ipsilateral normal ACA, ICA, and PCA velocities. Therefore, an elevation in the velocity (or corresponding ratio to ipsilateral exICA velocity) in any of these other arteries above thresholds validated for vasospasm in the MCA are very likely to represent vasospasm in those vessels as well; this is especially true when the mCBFV in any of these other arteries exceeds 200 cm/s. Normal velocities in the posterior circulation are typically lower than in the anterior circulation. In one study, a basilar velocity >85 cm/s and a ratio of basilar to extracranial (measured in the neck, not transforaminal) vertebral mCBFV >3 had 92 % sensitivity and 97 % specificity for basilar narrowing of more than 50 % on angiography [11]. While mCBFV identifies large vessel vasospasm and not tissue ischemia, a PI $\leq$ 0.58 may identify patients with large vessel vasospasm at higher risk for subsequent clinical neurological decline [12].

2. Determination of brain death
   The American Academy of Neurology's Quality Standards Subcommittee requires that the determination of brain death using TCD/TCCS be made on the basis of reverberating flow (Fig. 15.18) or short systolic spikes (Fig. 15.19) recorded in the anterior circulation (typically the MCA) bilaterally as well as in the posterior circulation (basilar) [1]. While the presence of such diffuse reverberating flow or short systolic spikes is considered incompatible with clinical recovery, the absence of flow signal cannot be used to determine brain death, since the inability to detect signal is commonly the result of inadequate windows or other technical factors.
3. Recanalization following acute ischemic stroke
   The spectral Doppler waveform obtained from the vessel targeted by reperfusion therapy, either intravenous tissue plasminogen activator (tPA) or endovascular therapy, may be used to assess the degree of recanalization. The consensus on grading intracranial flow obstruction (COGIF) score has been proposed as a tool for assessment of recanalization in clinical trials of acute ischemic stroke using TCCS and is shown in Table 15.2 [13].

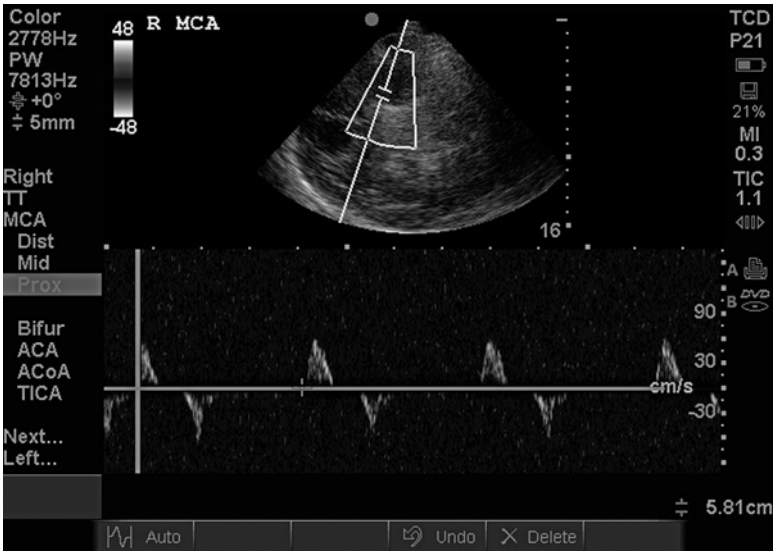

Fig. 15.18 Reverberating flow in brain death. Reverberating systolic/diastolic flow seen in the MCA. When present in both MCAs and the basilar, this is incompatible with clinical recovery

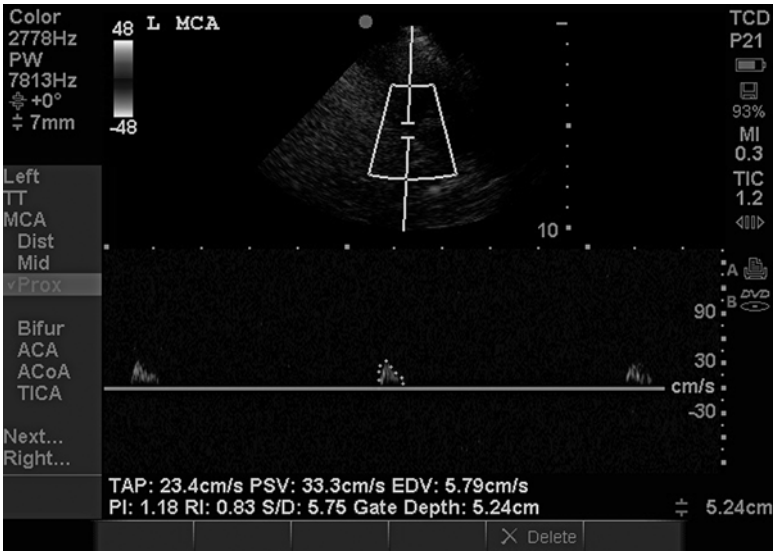

Fig. 15.19 Short systolic spikes in brain death. Short systolic spikes with no diastolic flow in the MCA. When present in both MCAs and the basilar, this is incompatible with clinical recovery

Table 15.2 Consensus on grading intracranial flow obstruction (COGIF) scale for assessment of recanalization following thrombolysis for acute ischemic stroke

COGIF grade	Hemodynamic pattern on TCCS	Clinical significance
1	No flow	Absent recanalization OR suboptimal acoustic window
2	Low systolic flow velocities, absent diastolic flow	Minimal recanalization OR downstream/ upstream severe narrowing or obstruction
3	Low systolic flow velocities with some diastolic flow	Partial recanalization OR downstream/ upstream severe narrowing or obstruction
4 Established perfusion		Established perfusion
(a) Flow velocities equal to contralateral side		Normal flow
(b) High focal flow velocities		Focal intracranial stenosis
(c) High segmental flow velocities		Hyperperfusion

Basic and Advanced Competencies in TCCS

There is, as yet, no consensus on what may constitute basic or core competencies in the performance and interpretation of TCCS in the neurointensive care unit. As the most common and well-established indication for TCCS in the neuroICU, the detection of vasospasm following aSAH would likely be considered a core competency, while the use of TCCS for brain death determination and assessment of recanalization are used less commonly than vasospasm monitoring and may therefore be considered relatively advanced competencies.

Evidence Review and Evidence-Based Use

Vasospasm of the large intracranial arteries evaluated by TCCS occurs in up to 70 % of patients with aneurysmal subarachnoid hemorrhage (aSAH) in a time window between 3 and 14 days following ictus (peak 8–10 days), although a majority of these patients remain asymptomatic [14–16]. About 20–30 % of patients will, however, develop delayed cerebral ischemia (DCI), presumably from severe vasospasm resulting in compromised distal flow to the brain, with 15–20 % of patients progressing to death or cerebral infarction [17–19]. Delayed infarction can result in severe morbidity and long-term functional disability [19].

The evidence that the use of TCD/TCCS is useful, although not definitive, for the prediction of large vessel (angiographic) vasospasm in the MCA following a SAH is robust [1, 10, 14, 15]. The predictive value appears to be substantially lower for vessels other than the MCA [10]. In one meta-analysis of 26 studies assessing the predictive value of TCD for vasospasm, sensitivity was 67 % (95 % CI 48–87 %), specificity 99 % (98–100 %), positive predictive value (PPV) 97 % (95–98 %), and

negative predictive value (NPV) 78 % (65–91 %) for the MCA. For the ACA, however, sensitivity was 42 % (11–72 %), specificity 76 % (53–100 %), PPV 56 % (27–84 %), and NPV 69 % (43–95 %) [10]. The frequency at which TCD/TCCS should be performed following aSAH is unclear, although many institutions perform daily TCD/TCCS evaluation while the patient is within the risk period for vasospasm.

In 2004, the Therapeutics and Technology Assessment Subcommittee of the American Academy of Neurology specified clinical indications for which the use of TCD/TCCS is well established on the basis of the existing evidence [1]. Detection and monitoring of large vessel vasospasm following aSAH was found to be a "setting in which TCD is able to provide information and in which its clinical utility is established," based on a moderately high level of evidence. In contrast, confirmation of cerebral circulatory arrest in the patient with suspected brain death was determined to be a "setting in which TCD is able to provide information, but in which its clinical utility, compared with other diagnostic tools, remains to be determined," while the monitoring of thrombolysis of acute MCA occlusions was determined to be a "setting in which TCD is able to provide information, but in which its clinical utility remains to be determined."

Pitfalls and Precautions

While considering the evidence base for the use of TCD/TCCS in prediction and monitoring of vasospasm following aSAH, several factors must be taken into account. While accurate at predicting large vessel vasospasm, TCD/TCCS is not consistently accurate at predicting the development of DCI and delayed infarction [20]. It is now recognized that DCI and angiographic vasospasm are distinct entities – patients with even severe angiographic vasospasm may continue to perfuse cerebral tissue adequately and DCI may occur in the absence of severe vasospasm [21]. The treatment of cerebral vasospasm with either hemodynamic augmentation or endovascular therapy, although widely performed, has not been evaluated in clinical trials with meaningful outcome measures. The presence of severe angiographic vasospasm, however, is strongly *correlated* with the subsequent occurrence of DCI [19], and the expectation that a severe reduction in luminal diameter will eventually compromise tissue perfusion is reasonable. The presence of TCCS evidence of severe vasospasm should, therefore, be a "red flag" that warrants close monitoring of the patient's hemodynamic and neurological condition, with hemodynamic and endovascular intervention considered for any neurological decline.

As previously mentioned, an important limitation in the use of TCCS is the relatively frequent (5–20 %) absence of adequate acoustic windows [7, 8]. As with any other ultrasound examination, TCCS is an operator-dependent tool and is prone to error in the hands of less experienced operators. The ACA in particular is often challenging to detect on duplex examination. Angle-corrected velocities obtained from

TCCS are significantly higher than those obtained from TCD and may lead to overestimation of vasospasm when using criteria established using "blind" TCD. Therefore, in the absence of large studies correlating angle corrected velocities to angiographic vasospasm, the University of Michigan protocol is to attempt to obtain as narrow an angle of insonation as possible using image guidance but not to perform angle-correction.

B-Mode Imaging of the Cerebral Parenchyma

While transcranial ultrasound is routinely used for the detection of intracranial hemorrhage in neonates, there has been interest more recently in the use of B-mode imaging of the cerebral parenchyma in adults, particularly when a decompressive craniectomy defect permits adequate acoustic transmission. Imaging of the cerebral parenchyma can be performed by first identifying the plane of the midbrain, as described above, then tilting the probe minimally upward/cephalad until the *third ventricle* and *lateral ventricles* are seen. This is typically possible only in the patients with the very best temporal acoustic windows, primarily patients with decompressive craniectomy and a large skull defect. While the lateral ventricles are hypoechoic from their fluid content, in the absence of hydrocephalus, it is the hyperechoic *choroid plexus* within the ventricles that is often visualized (Figs. 15.20 and 15.21).

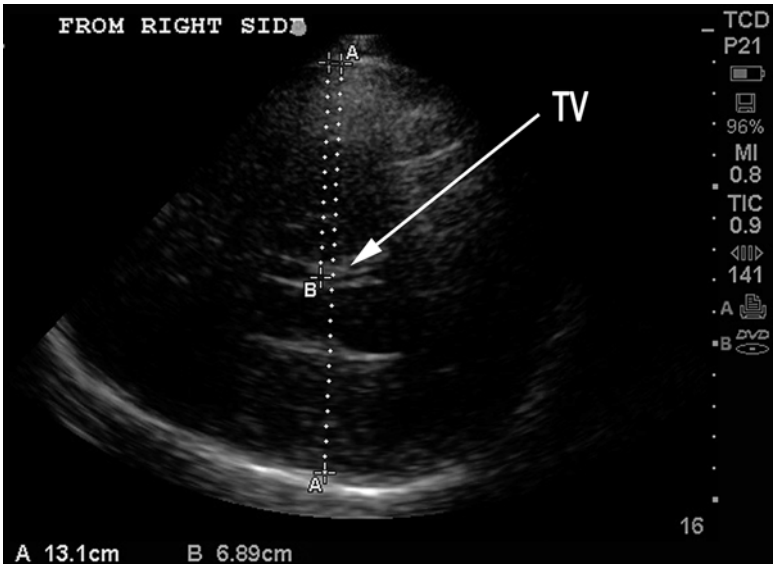

Fig. 15.20 B-mode measurement of midline shift – measurement from *right*. Patient with large right MCA infarction. Third ventricle (TV) is identified by the presence of the hyperechoic *double line* ("tram track") of the choroid plexus and marks the midline. Distance from surface to TV is 6.89 cm from the *right* and (see Fig. 15.21) 6.19 cm from the *left*. Midline shift is therefore (6.89–6.19)/2 = 0.35 cm, almost identical to the midline shift measured on CT (see Fig. 15.22)

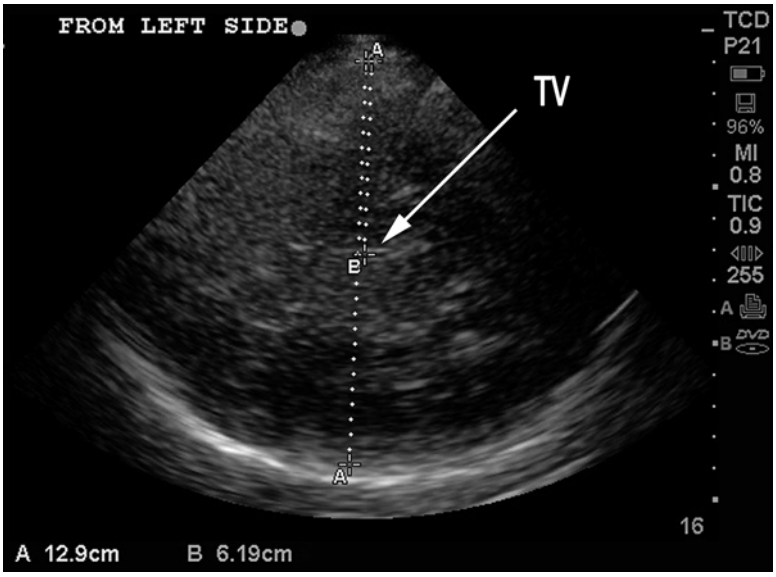

Fig. 15.21 B-mode measurement of midline shift – measurement from *left*. Patient with large right MCA infarction. Third ventricle (TV) is identified by the presence of the hyperechoic *double line* ("tram track") of the choroid plexus and marks the midline. Distance from surface to TV is 6.19 cm from the *left* and 6.89 cm from the *right* (see Fig. 15.20). Midline shift is therefore (6.89–6.19)/2 = 0.35 cm, almost identical to the midline shift measured on CT (see Fig. 15.22)

The third ventricle can be used to identify the *midline*, and *midline shift* in the setting of space-occupying lesions (such as malignant MCA infarction) is calculated as the difference in the distance from the probe to the midline from each side, divided by two (Figs. 15.20 and 15.21) with good correlation to measurement using CT (Fig. 15.22) [22]. Assessment using B-mode also has good correlation to CT imaging for determination of lateral ventricular size in hydrocephalus (Figs. 15.23 and 15.24) as well as for the detection and measurement of intraparenchymal hematomas (Figs. 15.25 and 15.26) [23, 24]. While B-mode imaging of the brain appears to hold significant promise, it is considered investigational at this time, and its clinical role not yet defined.

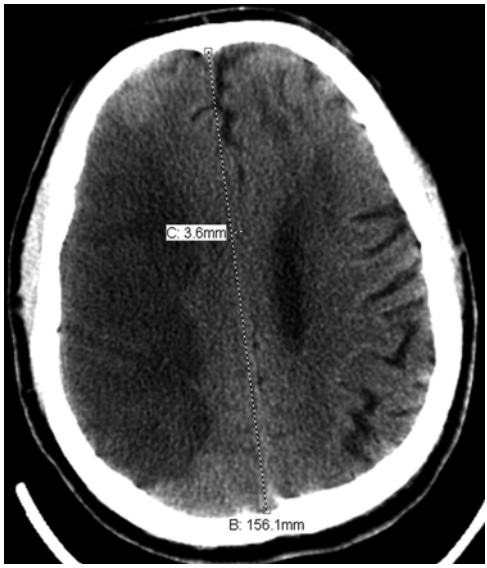

Fig. 15.22 CT measurement of midline shift. Same patient as in Figs. 15.20 and 15.21, same day as B-mode evaluation. Midline shift on CT (3.6 mm) is almost identical to midline shift calculated from B-mode imaging (see Figs. 15.20 and 15.21)

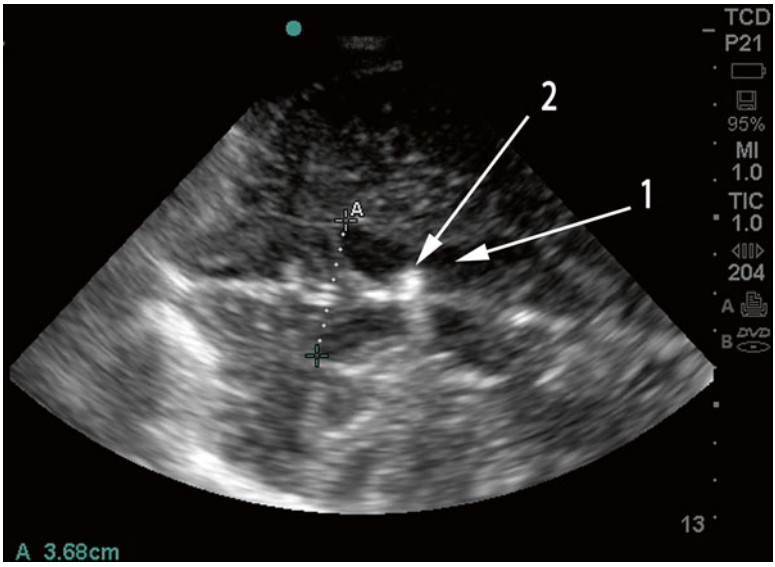

Fig. 15.23 Measurement of lateral ventricular size through craniectomy defect. Measurement of frontal horns for quantification of lateral ventricular size. Distance measured (3.68 cm) is almost identical to distance measured on CT (3.69 cm) in Fig. 15.24. *1* Right lateral ventricle, *2* external ventricular drain

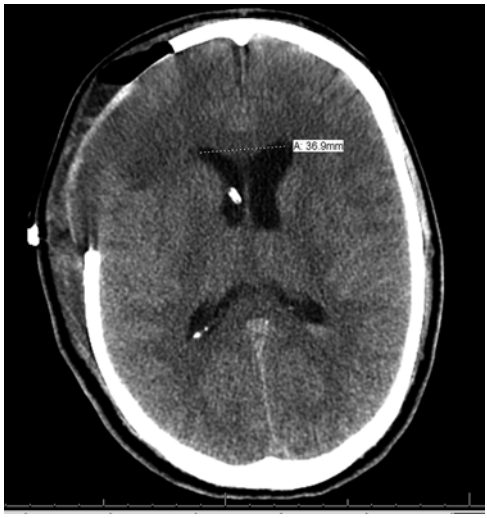

Fig. 15.24 Measurement of lateral ventricular size on CT. Same patient as in Fig. 15.23, on same day as B-mode examination. Distance measured (3.69 cm) is almost identical to distance measured on B-mode (3.68 cm) in Fig. 15.23. The external ventricular drain is seen in the same position in the right lateral ventricle as in Fig. 15.23

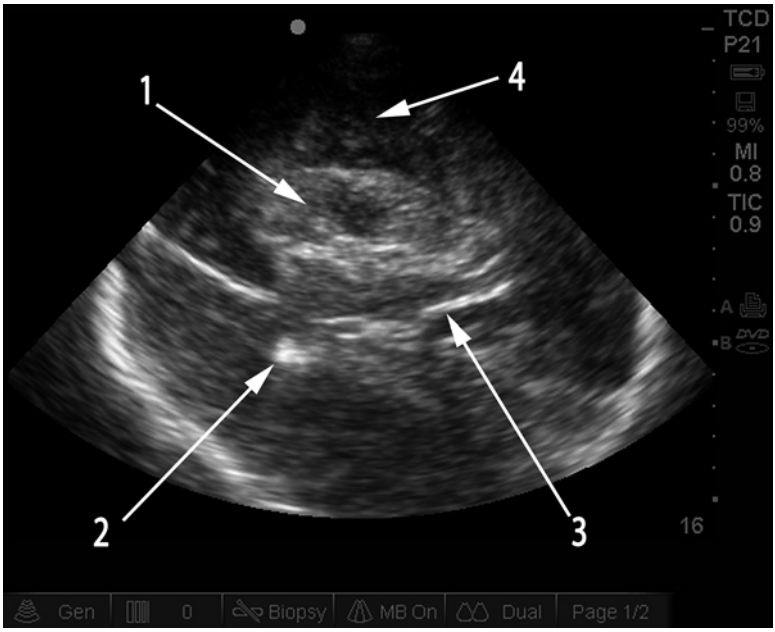

Fig. 15.25 B-mode for imaging of intracerebral hematoma through craniectomy defect. Large left hemispheric intracerebral hematoma (*1*). Compare to CT in Fig. 15.26 – same patient, same labeling. *2* External ventricular drain, *3* hyperechoic choroid plexus in left lateral ventricle, *4* skull defect

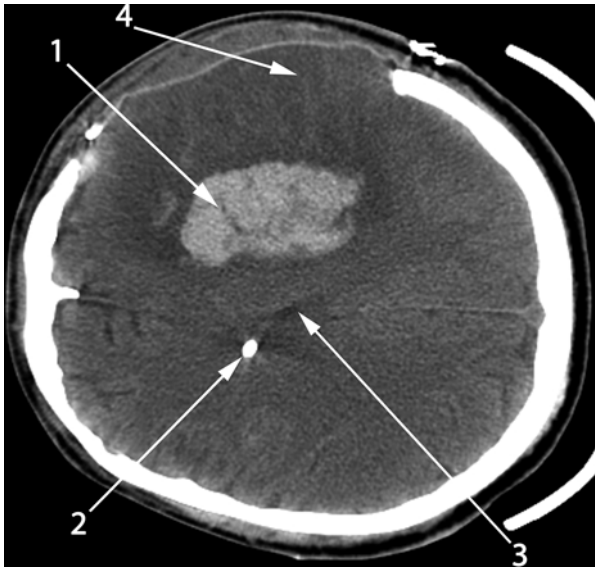

Fig. 15.26 Intracerebral hematoma on CT. Same patient as in Fig. 15.25, same day as B-mode evaluation. Same labeling. *1* hematoma, *2* external ventricular drain, *3* left lateral ventricle, *4* skull defect

Optic Nerve Ultrasound

Management of raised intracranial pressure is a cornerstone of patient management in the neuroICU. The assessment of ICP in a variety of acute neurological conditions typically requires the placement of an invasive monitor, either an external ventricular drain or a parenchymal catheter. Since there is expense and risk associated with the placement of invasive catheters, there is significant interest in potential techniques for the noninvasive detection of raised ICP. Of the available noninvasive techniques, ONUS appears to be among the most promising. The optic nerve sheath is a continuation of the dura and contains the subarachnoid space. An elevation in the ICP is transmitted down the subarachnoid space and results in distension of the optic nerve sheath (ONS), which can be detected using ocular ultrasound. While the same mechanism eventually results in papilledema, this can take hours or days, and papilledema can persist for hours to days following return of ICP to normal levels.

Technical and Patient Factors

Equipment

A linear array (13–6 MHz) transducer probe (Fig. 15.27) with an ophthalmic preset (Fig. 15.28) is recommended for this application, since not all probes and settings meet the Food and Drug Administration (FDA) requirements for ultrasound

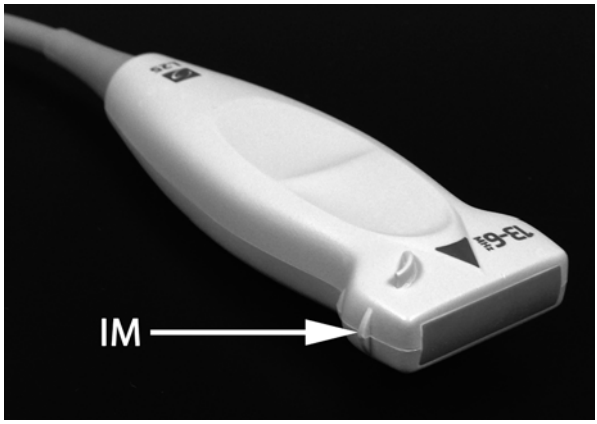

Fig. 15.27 Linear array transducer used for ONSD measurement. *IM* index mark on the probe, corresponds to index mark on the screen

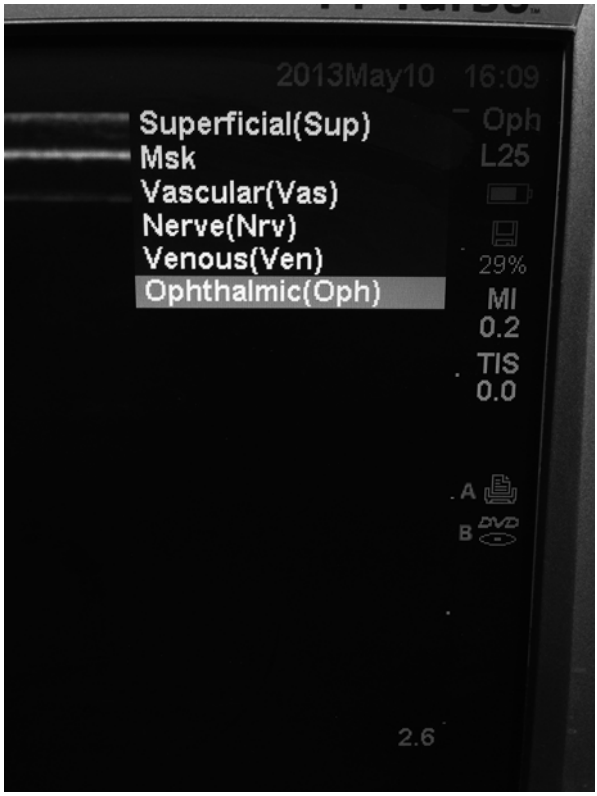

Fig. 15.28 Selection of ophthalmic preset. Select "Ophthalmic" from the list of presets available for the 13–6 MHz linear array transducer

examination of the eye. Theoretical concerns for thermal injury to the eye have led the FDA to limit the acoustic exposure during ocular ultrasound to a derated spatial-peak temporal-average intensity ($I_{SPTA.3}$) of $\leq$17 mW/cm^2 and mechanical index $\leq$0.23 [25].

Patient Factors

Patients with known optic nerve pathology or evident injury to the globe have typically been excluded from studies of ONUS [2–6].

Image Acquisition and Interpretation

Image Acquisition

The probe is placed on the superior and lateral aspect of the orbit against the upper eyelid, with the eye closed. The transducer is angled slightly caudally and medially (Fig. 15.29) until the *optic nerve* is visualized as a linear hypoechoic structure with clearly defined margins posterior to the globe (Fig. 15.30). The probe is never placed in direct contact with the cornea or sclera to avoid corneal abrasion. Contact with the eye must be gentle at all times, as excess pressure can result in nausea, vomiting, and a vagal response. The University of Michigan protocol is then to perform magnification and to use calipers to identify a point 3 mm behind the retina. The optic nerve sheath diameter (ONSD) is measured at this level using a second set of calipers. Very careful probe manipulation is performed to obtain clear margins of the ONS, distinct from the hypo- and hyper-echoic artifacts that are common posterior to the globe.

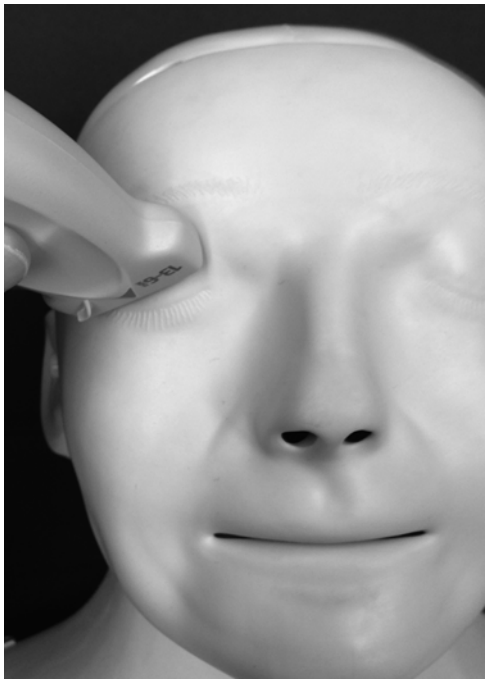

Fig. 15.29 Probe position for ONSD measurement. Transducer is placed on the *upper outer* margin of the orbit with the eye closed and angled slightly downward and medially

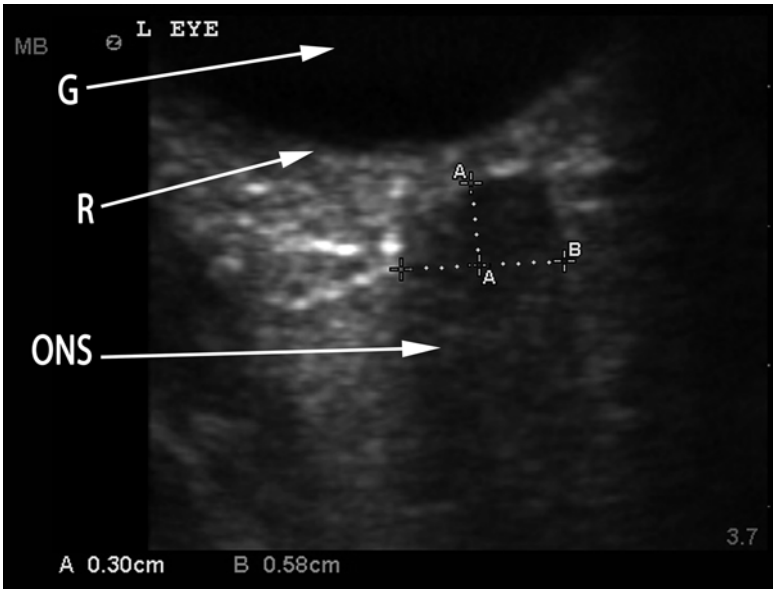

Fig. 15.30 ONSD measurement. The optic nerve sheath (ONS) is seen as a linear hypoechoic structure extending posterior to the globe (G). Caliper A measures a standard distance 3 mm behind the retina (R). Caliper B measures the ONSD at this level. ONSD is 0.58 cm, higher than the 0.50 cm cutoff. This patient was found to have ICP>40 mmHg following placement of an external ventricular drain

Image Interpretation

The optimal ONSD cutoff for the identification of raised intracranial pressure (ICP), typically defined as >20 mmHg, is a matter of debate. The validation study performed at the University of Michigan identified an optimal ONSD cutoff ≥0.50 cm for the detection of intracranial hypertension (defined as ICP>20 mmHg) with sensitivity 90 % (95 % CI 79–97 %), specificity 98 % (94–99 %), PPV 92 % (95 % CI 81–98 %), and NPV 97 % (93–99 %). For patients not on mechanical ventilation the optimal ONSD cutoff was ≥0.48 cm with sensitivity 99 % (93–100 %), specificity 95 % (91–97 %), PPV 85 % (76–92 %), and NPV 100 % (98–100 %).

Evidence Review and Evidence-Based Use

Several investigators have performed blinded correlation of ONSD measurement to the gold standard of simultaneous invasive ICP measurement [2–6]. These studies, as well as a subsequent meta-analysis, concluded that ONSD measurement was an accurate tool for the detection of raised ICP (>20 mmHg) [26]. The sensitivity of

this tool has ranged from 74 % to 96 % and specificity 74–99 % in different studies [2–6]. Agreement does NOT exist, however, on the optimal ONSD threshold for identification of raised ICP (>20 mmHg), with the suggested cutoff ranging from 0.48 cm to 0.58 cm. This variability may be related to variations in techniques of measurement and the presence of artifacts. In view of the discrepancy in the optimal ONSD threshold across studies, significant caution must be used in the interpretation of this test, unless validation of the specific technique being used at the clinician's institution against invasive ICP monitoring has been performed. Based on such a validation study [6] we use the cutoffs mentioned in the earlier section but always integrate ONSD measurement into a comprehensive clinical evaluation that includes history, physical examination, and imaging before decisions are made to treat intracranial hypertension. The presence of an ONSD above the threshold value should lead to consideration for the placement of an invasive ICP monitor.

Pitfalls and Precautions

The variation in optimal ONSD threshold for detection of elevated ICP has been discussed above. While this variation may be partly related to technique, it may also be related to the frequent presence of linear hypoechoic and hyperechoic artifacts posterior to the globe, which can significantly confound ONSD measurement. Figures 15.31 and 15.32 illustrate how inclusion of hypoechoic signal beyond the

Fig. 15.31 Artifact and ONSD – incorrect measurement. Inclusion of hyperechoic structures posterior to the globe other than the content of the optic nerve sheath can lead to serious error. In this case, ONSD is mistakenly measured at 0.64 cm, which would suggest a very high ICP. The ICP recorded from the external ventricular drain was only 11 mmHg

Fig. 15.32 Artifact and ONSD – correct measurement. Same examination as in Fig. 15.31. More careful measurement of only the content of the optic nerve sheath reveals ONSD is 0.38 cm, consistent with the normal ICP (11 mmHg) measured from the external ventricular drain

content of the ONS may result in misidentification of raised ICP. A delay in reversibility of ONS distension following a period of raised ICP may also possibly result in a decreased PPV in the setting of active treatment of raised ICP [27, 28]. Remember that ONUS is a qualitative (high vs normal) and not a quantitative assessment of ICP. Also, it is a snapshot assessment in time and not a continuous measure of ICP.

Cardiopulmonary Evaluation in Subarachnoid Hemorrhage

Technical considerations, image acquisition and interpretation of bedside echocardiography, and thoracic ultrasound have been described in detail elsewhere in this book. This section will briefly detail considerations specific to the neurointensive care unit.

Cardiomyopathy

Up to 30 % of patients with aSAH develop significant cardiac injury, with more severe grades of aSAH incrementally associated with more severe cardiac injury [29]. This injury may be a consequence of the catecholamine surge that accompanies

aSAH, leading to both acute endocardial and myocardial injury [30]. While cardiac injury can manifest as transient electrocardiogram changes or troponin elevation, severe left ventricular (LV) failure can occur, leading to cardiogenic shock and pulmonary edema. The occurrence of cardiac injury is also predictive of DCI, poor functional outcomes, and death [31].

Patients with aSAH and LV failure typically demonstrate a pattern similar to Takotsubo cardiomyopathy, with apical and/or mid-ventricular hypokinesia or akinesia and sparing of the basal segments [32]. Left ventricular dysfunction is typically maximal soon after ictus and almost always resolves over a period of days to weeks. Rapid identification of the severity and pattern of LV dysfunction in the setting of cardiogenic shock permits the initiation of appropriate therapy, including the addition of inotropic agents such as dobutamine or vasopressors such as norepinephrine.

Pulmonary Edema

Neurogenic pulmonary edema is relatively common following aSAH but may also occur in a range of acute neurological conditions [33]. Neurogenic edema is thought to result from an abrupt increase in pulmonary hydrostatic pressure and capillary permeability and can result in severe hypoxic respiratory failure but is transient and typically resolves over several days. Similar to cardiac injury, the incidence and severity is highest at admission. The use of thoracic ultrasound can be very valuable for the diagnosis of acute pulmonary edema. Using the "BLUE" (bedside lung ultrasound in emergency) protocol for assessment of respiratory failure, the presence of bilateral B-lines in the anterior fields in the patient with aSAH likely suggests the presence of aSAH (Fig. 15.33) [34].

Hemodynamic Augmentation for DCI

The mainstay of treatment of DCI along with endovascular therapy is hemodynamic augmentation to promote perfusion of ischemic cerebral tissue. The use of ultrasound can be helpful in this regard, allowing for assessment of volume status and optimization of cardiac output. The presence of complete end-systolic obliteration of the left ventricular cavity implies significant hypovolemia and the need for fluid resuscitation (Fig. 15.34) [35]. Respiratory variation in the inferior vena cava (IVC) diameter is a useful predictor of fluid responsiveness in the patient on the ventilator without respiratory effort [36]. When severe LV dysfunction is identified on echocardiography, the addition of dobutamine to vasopressors may be valuable in promoting cerebral perfusion [37]. Inotropic therapy and fluid resuscitation can be titrated to the measured stroke volume, obtained either by the fractional shortening

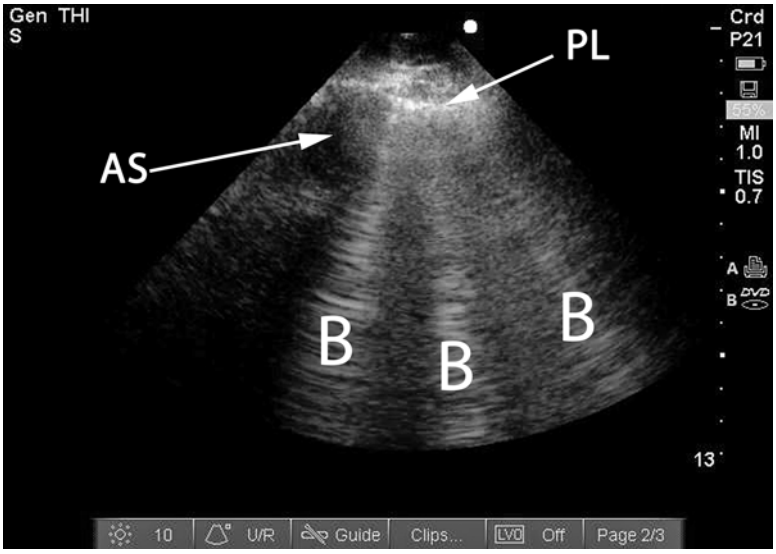

Fig. 15.33 B-lines on thoracic ultrasound. Patient with SAH and severe neurogenic pulmonary edema. *PL* pleural line, *AS* acoustic shadow of rib, *B* B-lines, extending from pleural line to edge of screen

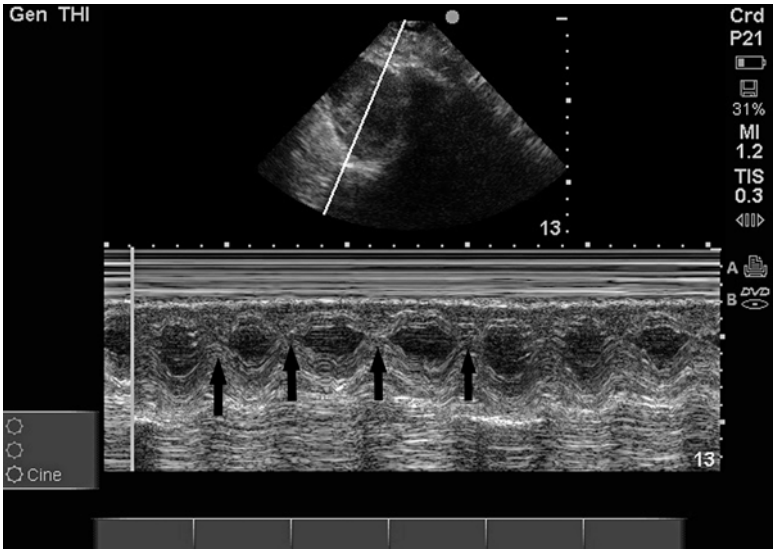

Fig. 15.34 Echocardiography M-mode demonstrating hypovolemia. Patient with aSAH, cerebral salt wasting, and delayed cerebral ischemia. M-mode examination performed in the parasternal short axis view at the papillary muscle level. *Black vertical arrows* demonstrate end-systolic obliteration of the left ventricular cavity, suggesting significant hypovolemia and the need for fluid resuscitation

method or by measurement of LV outflow tract diameter and aortic valve Doppler, both of which are described elsewhere in this book. While performing fluid resuscitation for DCI, the appearance of new B-lines bilaterally on thoracic ultrasound may be useful in the early identification of fluid overload and pulmonary edema.

Other Applications of Ultrasound in the Neuro-ICU

Similar to their use in other ICUs, the following applications of bedside ultrasound find common use in the neuroICU:

1. Echocardiography for assessment of shock and preload
2. Measurement of IVC for assessment of fluid responsiveness
3. Thoracic ultrasound for the assessment of acute respiratory failure ("BLUE" protocol)
4. Extended focused assessment with sonography in trauma (eFAST) for patients with severe traumatic brain injury and multisystem injuries
5. Diagnosis of deep vein thrombosis
6. Real-time guidance for bedside procedures: central venous and arterial catheterization, thoracentesis, paracentesis, and percutaneous tracheostomy

Conclusion

While TCD has long been an integral part of evaluation and management of patients with acute brain injury, more recently the range of applications of ultrasound in the ICU have greatly expanded. Gaining proficiency in all aspects of critical care ultrasound is likely to empower the neurointensivist to significantly enhance the range and depth of clinical care provided to patients in the neuroICU.

References

1. Sloan MA, Alexandrov AV, Tegeler CH, Spencer MP, Caplan LR, Feldmann E, Wechsler LR, Newell DW, Gomez CR, Babikian VL, Lefkowitz D, Goldman RS, Armon C, Hsu CY, Goodin DS, Therapeutics and Technology Assessment Subcommittee of the American Academy of Neurology. Assessment: transcranial Doppler ultrasonography: report of the therapeutics and technology assessment subcommittee of the American academy of neurology. Neurology. 2004;62(9):1468–81.
2. Geeraerts T, Launey Y, Martin L, Pottecher J, Vigué B, Duranteau J, Benhamou D. Ultrasonography of the optic nerve sheath may be useful for detecting raised intracranial pressure after severe brain injury. Intensive Care Med. 2007;33(10):1704–11. Epub 2007 Aug 1.
3. Kimberly HH, Shah S, Marill K, Noble V. Correlation of optic nerve sheath diameter with direct measurement of intracranial pressure. Acad Emerg Med. 2008;15(2):201–4.

4. Soldatos T, Karakitsos D, Chatzimichail K, Papathanasiou M, Gouliamos A, Karabinis A. Optic nerve sonography in the diagnostic evaluation of adult brain injury. Crit Care. 2008;12(3):R67. Epub 2008 May 13.
5. Moretti R, Pizzi B, Cassini F, Vivaldi N. Reliability of optic nerve ultrasound for the evaluation of patients with spontaneous intracranial hemorrhage. Neurocrit Care. 2009;11(3):406–10.
6. Rajajee V, Vanaman M, Fletcher JJ, Jacobs TL. Optic nerve ultrasound for the detection of raised intracranial pressure. Neurocrit Care. 2011;15(3):506–15.
7. Krejza J, Swiat M, Pawlak MA, Oszkinis G, Weigele J, Hurst RW, Kasner S. Suitability of temporal bone acoustic window: conventional TCD versus transcranial color-coded duplex sonography. J Neuroimaging. 2007;17(4):311–4.
8. Wijnhoud AD, Franckena M, van der Lugt A, Koudstaal PJ, Dippel ED. Inadequate acoustical temporal bone window in patients with a transient ischemic attack or minor stroke: role of skull thickness and bone density. Ultrasound Med Biol. 2008;34(6):923–9. doi:10.1016/j.ultrasmedbio.2007.11.022. Epub 2008 Feb 20.
9. Alexandrov AV, Neumyer MM. Practical models of cerebral hemodynamics and waveform recognition. In: Alexandrov A, editor. Cerebrovascular ultrasound in stroke prevention and treatment. 1st ed. Elmsford: Blackwell publishing; 2004. p. 66.
10. Lysakowski C, Walder B, Costanza MC, Tramer MR. Transcranial Doppler versus angiography in patients with vasospasm due to a ruptured cerebral aneurysm: a systematic review. Stroke. 2001;32:2292–8.
11. Sviri GE, Ghodke B, Britz GW, Douville CM, Haynor DR, Mesiwala AH, Lam AM, Newell DW. Transcranial Doppler grading criteria for basilar artery vasospasm. Neurosurgery. 2006;59(2):360–6; discussion 360–6.
12. Rajajee V, Fletcher JJ, Pandey AS, Gemmete JJ, Chaudhary N, Jacobs TL, Thompson BG. Low pulsatility index on transcranial Doppler predicts symptomatic large-vessel vasospasm after aneurysmal subarachnoid hemorrhage. Neurosurgery. 2012;70(5):1195–206; discussion 1206.
13. Nedelmann M, Stolz E, Gerriets T, Baumgartner RW, Malferrari G, Seidel G, Kaps M, TCCS Consensus Group. Consensus recommendations for transcranial color-coded duplex sonography for the assessment of intracranial arteries in clinical trials on acute stroke. Stroke. 2009;40(10):3238–44.
14. Connolly Jr ES, Rabinstein AA, Carhuapoma JR, Derdeyn CP, Dion J, Higashida RT, Hoh BL, Kirkness CJ, Naidech AM, Ogilvy CS, Patel AB, Thompson BG, Vespa P, American Heart Association Stroke Council, Council on Cardiovascular Radiology and Intervention, Council on Cardiovascular Nursing, Council on Cardiovascular Surgery and Anesthesia, Council on Clinical Cardiology. Guidelines for the management of aneurysmal subarachnoid hemorrhage: a guideline for healthcare professionals from the American Heart Association/American Stroke Association. Stroke. 2012;43(6):1711–37.
15. Diringer MN, Bleck TP, Claude Hemphill 3rd J, Menon D, Shutter L, Vespa P, Bruder N, Connolly Jr ES, Citerio G, Gress D, Hänggi D, Hoh BL, Lanzino G, Le Roux P, Rabinstein A, Schmutzhard E, Stocchetti N, Suarez JI, Treggiari M, Tseng MY, Vergouwen MD, Wolf S, Zipfel G, Neurocritical Care Society. Critical care management of patients following aneurysmal subarachnoid hemorrhage: recommendations from the Neurocritical Care Society's Multidisciplinary Consensus Conference. Neurocrit Care. 2011;15(2):211–40.
16. Fisher CM, Roberson GH, Ojemann RG. Cerebral vasospasm with ruptured saccular aneurysm: the clinical manifestations. Neurosurgery. 1977;1:245–8.
17. Haley Jr EC, Kassell NF, Torner JC. The international cooperative study on the timing of aneurysm surgery: the North American experience. Stroke. 1992;23:205–14.
18. Longstreth Jr WT, Nelson LM, Koepsell TD, van Belle G. Clinical course of spontaneous subarachnoid hemorrhage: a population-based study in King County, Washington. Neurology. 1993;43:712–8.
19. Frontera JA, Fernandez A, Schmidt JM, Claassen J, Wartenberg KE, Badjatia N, Connolly ES, Mayer SA. Defining vasospasm after subarachnoid hemorrhage: what is the most clinically relevant definition? Stroke. 2009;40:1963–8.

20. Carrera E, Schmidt JM, Oddo M, Fernandez L, Claassen J, Seder D, Lee K, Badjatia N, Connolly Jr ES, Mayer SA. Transcranial Doppler for predicting delayed cerebral ischemia after subarachnoid hemorrhage. Neurosurgery. 2009;65:316–23.
21. Dankbaar JW, Rijsdijk M, van der Schaaf IC, Velthuis BK, Wermer MJ, Rinkel GJ. Relationship between vasospasm, cerebral perfusion, and delayed cerebral ischemia after aneurysmal subarachnoid hemorrhage. Neuroradiology. 2009;51:813–9.
22. Stolz E, Gerriets T, Fiss I, Babacan SS, Seidel G, Kaps M. Comparison of transcranial color-coded duplex sonography and cranial CT measurements for determining third ventricle midline shift in space-occupying stroke. AJNR Am J Neuroradiol. 1999;20(8):1567–71.
23. Becker G, Bogdahn U, Strassburg HM, Lindner A, Hassel W, Meixensberger J, Hofmann EJ. Identification of ventricular enlargement and estimation of intracranial pressure by transcranial color-coded real-time sonography. Neuroimaging. 1994;4(1):17–22.
24. Kukulska-Pawluczuk B, Książkiewicz B, Nowaczewska M. Imaging of spontaneous intracerebral hemorrhages by means of transcranial color-coded sonography. Eur J Radiol. 2012;81(6):1253–8.
25. Guidance for industry and FDA staff – information for manufacturers seeking marketing clearance of diagnostic ultrasound systems and transducers. 2008. http://www.fda.gov/medicaldevices/deviceregulationandguidance/guidancedocuments/ucm070856.htm
26. Dubourg J, Javouhey E, Geeraerts T, Messerer M, Kassai B. Ultrasonography of optic nerve sheath diameter for detection of raised intracranial pressure: a systematic review and meta-analysis. Intensive Care Med. 2011;37(7):1059–68.
27. Hansen HC, Lagrèze W, Krueger O, Helmke K. Dependence of the optic nerve sheath diameter on acutely applied subarachnoidal pressure – an experimental ultrasound study. Acta Ophthalmol. 2011;89(6):e528–32.
28. Rajajee V, Fletcher JJ, Rochlen LR, Jacobs TL. Comparison of accuracy of optic nerve ultrasound for the detection of intracranial hypertension in the setting of acutely fluctuating vs stable intracranial pressure: post-hoc analysis of data from a prospective, blinded single center study. Crit Care. 2012;16(3):R79.
29. Hravnak M, Frangiskakis JM, Crago EA, Chang Y, Tanabe M, Gorcsan 3rd J, Horowitz MB. Elevated cardiac troponin I and relationship to persistence of electrocardiographic and echocardiographic abnormalities after aneurysmal subarachnoid hemorrhage. Stroke. 2009;40(11):3478.
30. Hinson HE, Sheth KN. Manifestations of the hyperadrenergic state after acute brain injury. Curr Opin Crit Care. 2012;18(2):139–45.
31. van der Bilt IA, Hasan D, Vandertop WP, Wilde AA, Algra A, Visser FC, Rinkel GJ. Impact of cardiac complications on outcome after aneurysmal subarachnoid hemorrhage: a meta-analysis. Neurology. 2009;72(7):635.
32. Lee VH, Connolly HM, Fulgham JR, Manno EM, Brown Jr RD, Wijdicks EF. Tako-tsubo cardiomyopathy in aneurysmal subarachnoid hemorrhage: an underappreciated ventricular dysfunction. J Neurosurg. 2006;105(2):264.
33. Baumann A, Audibert G, McDonnell J, Mertes PM. Neurogenic pulmonary edema. Acta Anaesthesiol Scand. 2007;51:447.
34. Lichtenstein DA, Mezière GA. Relevance of lung ultrasound in the diagnosis of acute respiratory failure: the BLUE protocol. Chest. 2008;134(1):117–25. Epub 2008 Apr 10.
35. Leung JM, Levine EH. Left ventricular end-systolic cavity obliteration as an estimate of intraoperative hypovolemia. Anesthesiology. 1994;81(5):1102–9.
36. Barbier C, Loubières Y, Schmit C, Hayon J, Ricôme JL, Jardin F, Vieillard-Baron A. Respiratory changes in inferior vena cava diameter are helpful in predicting fluid responsiveness in ventilated septic patients. Intensive Care Med. 2004;30(9):1740–6. Epub 2004 Mar 18.
37. Joseph M, Ziadi S, Nates J, Dannenbaum M, Malkoff M. Increases in cardiac output can reverse flow deficits from vasospasm independent of blood pressure: a study using xenon computed tomographic measurement of cerebral blood flow. Neurosurgery. 2003;53(5):1044–51; discussion 1051–2.